doi:10.26443/seismica.v4i2.1690

SEISMICA

Improving microearthquake detection in the Val d'Agri region (Southern Italy) with deep learning

Elisa Caredda * [1], **Marius Paul Isken**[3], **Simone Cesca**[3], **Maddalena Errico**[2], **Giampaolo Zerbinato**[2], **Andrea Morelli**[2,1]

[1]*Dipartimento di Fisica e Astronomia "Augusto Righi" (DIFA), Alma Mater Studiorum Università di Bologna, Viale Berti Pichat 8, 40127 Bologna, Italy,* [2]*Istituto Nazionale di Geofisica e Vulcanologia, Sezione di Bologna, Viale Berti Pichat 6/2, 40127 Bologna, Italy,* [3]*GFZ Helmholtz Centre for Geosciences, Potsdam, Germany*

Author contributions: *Conceptualization*: Andrea Morelli, Elisa Caredda. *Methodology*: Elisa Caredda, Marius P. Isken, Simone Cesca, Andrea Morelli. *Software*: Elisa Caredda, Marius P. Isken. *Data Collection*: Maddalena Errico, Giampaolo Zerbinato. *Formal Analysis*: Elisa Caredda. *Writing - Original draft*: Elisa Caredda, Andrea Morelli, Simone Cesca. *Writing - Review & Editing*: Elisa Caredda, Andrea Morelli, Simone Cesca, Marius P. Isken, Maddalena Errico, Giampaolo Zerbinato. *Visualization*: Elisa Caredda, Andrea Morelli, Simone Cesca, Marius P. Isken, Maddalena Errico, Giampaolo Zerbinato. *Supervision*: Andrea Morelli, Simone Cesca.

Abstract The detection and monitoring of low-magnitude earthquakes are crucial for situational awareness and risk assessment. We employ two advanced methodologies for seismic arrival time picking, detection, and localization of microseismicity in the Basilicata region (southern Italy). Both approaches rely on deep neural networks for detecting and picking P- and S-wave arrivals. This region exhibits complex seismicity due to tectonic setting, reservoir impoundment, and hydrocarbon extraction, as it hosts Europe's largest onshore oil field and a dammed water reservoir. We compare our results with a reference catalog based on the classical short-time average over long-time average (STA/LTA) method and analyst reviews. The machine-learning-based catalogs identify approximately twice as many earthquakes as the reference bulletin, with recall rates (indicating the proportion of retrieved events also present in the reference catalog) of 93% and 77%, respectively. Our findings demonstrate that deep learning significantly improves the magnitude detection threshold while ensuring high reliability. A significant advantage is the fully automated and rapid workflow, which produces a homogeneous catalog and can be integrated into near-real-time seismic monitoring. These tools thus provide valuable advancements in earthquake detection and sequence analysis.

Production Editor:
Andrea Llenos
Handling Editor:
Hongyu Sun
Copy & Layout Editor:
Ethan Williams

Received:
8 April 2025
Accepted:
21 September 2025
Published:
3 November 2025

1 Introduction

Monitoring microseismicity is necessary for understanding and mitigating seismic hazard, particularly in regions that host hydrocarbon extraction, geothermal energy production, and other mining operations. High-resolution seismic monitoring allows the detection of small earthquakes that can provide valuable insights into the evolution of subsurface processes, fault mechanics, and the potential for larger seismic events (e.g., Fonzetti et al., 2024). While effective, traditional methods of seismic phase detection and event location are often challenged by the low signal-to-noise ratio (SNR) inherent to records of low-magnitude earthquakes.

Recent advances in deep learning have significantly expanded the range of tools available for seismic monitoring. For instance, EQTransformer employs an attention-based multitask architecture for joint phase picking and event detection, leading to substantial improvements in catalog completeness (Mousavi et al., 2020). Similarly, QuakeFlow integrates PhaseNet and GaMMA into a scalable, cloud-based workflow for efficient earthquake cataloging (Zhu et al., 2022a; Zhu and Beroza, 2019; Zhu et al., 2022b). The development of frameworks such as SeisBench further supports the standardization and benchmarking of machine learning models, including PhaseNet and EQTransformer (Woollam et al., 2022).

In addition to event detection and picking, Bayesian deep learning approaches have been proposed for estimating earthquake source parameters and their uncertainties from single-station recordings (Mousavi and Beroza, 2020). A recent review by Mousavi and Beroza (2023a) underscores the wide applicability of machine learning across the entire seismic workflow—from detection and picking to event clustering, focal mechanism analysis, and ground-motion prediction—while highlighting the importance of open data and standardized evaluation practices.

Among these tools, PhaseNet (Zhu and Beroza, 2019) is a neural network architecture standing out for its reliability in automatically detecting and picking seismic first arrivals in continuous waveform data, making it an invaluable tool for seismic monitoring for seismic monitoring. Integrating advanced neural network algorithms and robust location techniques represents a significant step forward in seismic monitoring.

The Val d'Agri area in Southern Italy hosts industrial activities related to oil extraction and wastewater reinjection in the largest European onshore reservoir, that is located in a tectonically active extensional regime (e.g., Cello et al., 2003) where an artificial water reservoir is also in operation (e.g. Valoroso et al., 2023). To ensure

*Corresponding author: elisa.caredda2@unibo.it

public safety and sustain industrial operations (Braun et al., 2020), the Val d'Agri region is subject to continuous seismic and geodetic monitoring. Since 2019 the CMS (Centro di Monitoraggio delle attività di Sottosuolo) — part of the INGV (Istituto Nazionale di Geofisica e Vulcanologia) — has the duty of operational seismic monitoring. Currently, routine monitoring operations require a manual check of results of the SeisComP software (Seiscomp, https://www.seiscomp.de/, last accessed on July 10, 2024), daily performed by operators (Morelli et al., 2025). The picking method employed by the software is based on implementing the STA/LTA ratio, which compares the energy changes in a short time window (STA) to those in a long time window (LTA). A potential seismic event is detected when the ratio of STA to LTA exceeds a predefined threshold (Allen, 1978). This is perhaps the most robust and commonly used method for the detection (and time-picking) of seismic arrivals in ground motion waveforms — its performance has been compared with that of other techniques (e.g., Vaezi and van der Baan, 2015).

Here we describe two methods based on deep learning (PhaseNet and Qseek, Zhu and Beroza, 2019; Isken et al., 2025) for arrival-time picking to study microseismicity in the Basilicata region in Southern Italy. Qseek (Isken et al., 2025) is a data-driven method that combines phase arrival annotations from pre-trained neural networks with waveform stacking and an adaptive octree search algorithm to detect and locate earthquakes automatically. We compare the performance of two neural network-based workflows against the reference catalog obtained using a conventional STA/LTA algorithm revised by the CMS-INGV operators. The operators manually check every detection and repick the phase arrivals when necessary. This study will assess the effectiveness of machine learning in detecting and locating microseismic events, highlighting its potential for improving seismic hazard assessment and risk mitigation in regions with widespread seismicity and industrial activities.

2 Data

The reference data consists of continuous velocity records from 56 stations belonging to various networks (GE, IV, IX, TP, VA, VD) covering an area of approximately 6500 km^2. Some stations are part of the INGV National Network (IV, https://doi.org/10.13127/sd/x0fxnh7qfy), GEOFON Seismic Network (GE, https://doi.org/10.14470/TR560404), CNR-IMAA High Agri Valley geophysical Observatory (VD, https://doi.org/10.7914/SN/VD, Stabile et al., 2020), ISNet - Irpinia Seismic Network (IX, https://www.fdsn.org/networks/detail/IX/). While other networks have been installed by private companies: VA (ENI SpA, 2001, https://doi.org/10.7914/SN/VA), and TP (TOTAL E&P Italia Spa, 2018, https://www.fdsn.org/networks/detail/TP/).

For each station, for each component (one vertical and two horizontal), we select one of the channels HH, EH or CH (sampling rates 100 to 250 Hz), in this prioritizing order, depending on availability. We analyse data from January 2021 to October 2023 (33 months). We employ the earthquake bulletin from CMS monitoring operations as a reference catalog. It has been obtained using the STA/LTA algorithm, with detections revised daily by operators. It contains 5,030 earthquakes in the selected period, with a local magnitude range from -1.1 to 3.8.

3 Methods

PRN workflow

We refer to the first of the two workflows as PRN after the names of the software here employed (PhaseNet, Real, NonLinLoc: Zhu and Beroza, 2019; Zhang et al., 2019; Lomax et al., 2000). In this workflow, we apply a bandpass filter between 1 and 45 Hz to the seismograms. This frequency range is chosen to maximize signal retention while enhancing the recall rate of seismic phase detection, particularly for micro-earthquakes, which radiate significant energy at high frequencies. The upper bound is constrained by the Nyquist frequency (given the 100 Hz sampling rate required b PhaseNet), while the lower bound helps suppress low-frequency noise. This choice also reflects common practice in similar studies (e.g., Mousavi et al., 2020; Wickham-Piotrowski et al., 2023), supporting its general applicability and reproducibility.

We use the PhaseNet original model and set the PhaseNet pick score (a pseudo-probability) threshold to 0.3 for the P and S phase arrivals to filter out low-confidence picks. This value was chosen based on empirical tests on our dataset and is consistent with thresholds adopted in previous studies using PhaseNet (e.g., Zhu and Beroza, 2019). This threshold offers a good balance between minimizing false picks and retaining valid arrivals, especially in low-SNR conditions. Although a PhaseNet variant trained on the Italian INSTANCE dataset (Michelini et al., 2021) exists, a recent comparative study in the Central Apennines (Cianetti et al., 2025) showed only marginal improvements over the original model. Given the similar tectonic context and waveform characteristics, we expect comparable performance in our study area and therefore opted for the original model. We apply the phase association algorithm REAL (Rapid Earthquake Association and Location; Zhang et al., 2019), with the requirement of a minimum of 7 phase arrivals per earthquake (at least 4 P phases, 3 S phases, and three stations with both P and S phases). We chose this threshold because it is a good compromise between reducing false positives and detecting small earthquakes. Furthermore, we apply a slightly more restrictive threshold compared to the CMS catalog, which uses a minimum number of 5. Since PhaseNet is more sensitive than STA/LTA method and generally provides a higher number of picks for the same event, we opted for a higher threshold to ensure robustness and reduce the inclusion of low-quality detections.

We set the maximum allowed residual for the preliminary locations computed by REAL to 2 seconds in order to include a larger number of candidate events during the initial phase association step. This approach is particularly useful when working with low-magnitude events, where stricter residual thresholds might exclude valid detections. Unlike NonLinLoc, REAL does not employ a detailed velocity model but rather uses constant P- and S-wave velocities, which justifies adopting more permissive residual limits at this stage.

S arrivals without a corresponding P arrival at the same station for the same event are discarded because they are generally less reliable.

After phase association, we use NonLinLoc software (Lomax et al., 2000, 2014) to solve for the absolute hypocentral location of the seismic events, assuming the same 1-D layered velocity model (Improta et al., 2017) used to generate the reference catalog, to ease comparison. NonLinLoc estimates the posterior probability density function of the hypocenter spatial location (Lomax et al., 2000, 2014). This workflow yields 21,617 earthquake locations.

To assess the reliability of the detections, we manually inspected a representative subset of 100 randomly selected events. Of these, 52 were confirmed as true earthquakes with reliable hypocentral solutions, yielding a precision of ~52% at this stage. Among the rejected events, some correspond to earthquakes located outside the study area, while others are characterized by very low signal-to-noise ratios, making a clear visual confirmation difficult.

We run NonLinLoc a second time, considering P and S wave station-specific delays, derived from the average residuals after the first run (Lomax et al., 2000, 2014). This improves location accuracy by reducing travel-time uncertainties. To filter out poor locations, events with horizontal and vertical uncertainties larger than 5 km, and those with RMS larger than 1 s are removed. Such tuning offers a good compromise: it reduces the number of false positives and bad associations while preserving a high recall rate. However, the new catalog does not include a small number of earthquakes from the original catalog due to the conservative thresholds used to filter out bad associations and locations.

Finally, we calculate the local magnitude M_L using the attenuation formula by Bakun and Joyner (1984):

$$M_L = log_{10}A + log_{10}\frac{r}{100} + 0.00301(r - 100) + 3 \quad (1)$$

where A is the amplitude in mm of the simulated record of a Wood-Anderson seismometer, and r is the epicentral distance in km. We use this equation because it is the same local magnitude (ML) relationship adopted for the reference CMS catalog for the Val d'Agri region. Although originally developed for Californian data, this relationship was chosen by the CMS team as a practical proxy for ML in this specific region (Morelli et al., 2025). Therefore, we apply the same formula to ensure consistency and comparability with the reference catalog. To calculate the magnitude, we first deconvolve the instrument response, simulate the corresponding Wood-Anderson response, and calculate amplitude A as the mean of the two horizontal half peak-to-peak amplitudes in mm of the recordings for each triggered station. The peak-to-peak amplitude is calculated within a window that starts 0.5 seconds before the P-wave arrival and ends 3 seconds after the expected S-wave arrival time. If only a P pick is available, the S arrival is estimated approximately using constant P and S velocities ($V_p = 6$ km /s and $V_s = 3.5$ km /s, typical values for the crust (Dziewonski and Anderson, 1981)) as $t_s \approx t_p + \Delta(\frac{1}{V_s} - \frac{1}{V_p})$, where Δ is the hypocentral distance. The final local magnitude is calculated as the median of all station magnitudes. The results are compared to the reference CMS (INGV) catalog.

To reassess the reliability after the refinements, we manually inspected a new subset of 100 randomly selected events. This analysis indicates that 88% of the detections correspond to true earthquakes with reliable hypocentral solutions, demonstrating a substantial improvement in precision compared to the first evaluation. This value reflects the intended balance between completeness and precision.

QS workflow

This workflow employs the *Qseek* (QS) framework (Isken et al., 2025), an automatic and data-driven earthquake detector and locator. This workflow employs neural network phase arrival annotations and waveform stacking for detection and localisation of seismicity using an adaptive octree grid search. We use PhaseNet (with the original model) for P and S first arrival picking. The location accuracy is further improved by applying source-specific station corrections, which can account for the 3D velocity heterogeneities (Isken et al., 2025; Richards-Dinger and Shearer, 2000).

Stacking-and-migration-based methods utilize the full waveform information. Stacking the arrivals enhances the signal-to-noise ratio (SNR) and allows for assessing the coherence of phase picks across multiple stations. Coherent energy from true seismic arrivals is reinforced, while incoherent noise is suppressed. The subsequent migration step backprojects the seismic energy toward the source (hypocenter) using the full shape of the phase arrival annotation (Isken et al., 2025). The stacked energy is defined as the semblance (Grigoli et al., 2014) measuring the seismic arrivals' alignment across multiple stations. It quantifies the coherence of signals by analyzing their energy distribution over time and space. The semblance of the stacked waveforms reaches the highest value at the hypocentral location. According to this definition, a higher semblance value increases the likelihood of detecting a true positive. To identify coherent seismic sources, we compute the maximum semblance over time and apply a detection threshold based on the Median Absolute Deviation (MAD) of this trace. The MAD is a robust measure of variability that allows us to adapt to varying noise levels. The MAD is scaled by a factor of 10 as a solid threshold value for the semblance. Although semblance is primarily a measure of the coherence of pick confidence across stations, it is also influenced by the signal-to-noise ratio (SNR) and data quality. For smaller events, especially those distant from the network, low SNR and fewer picks at some stations tend to reduce semblance

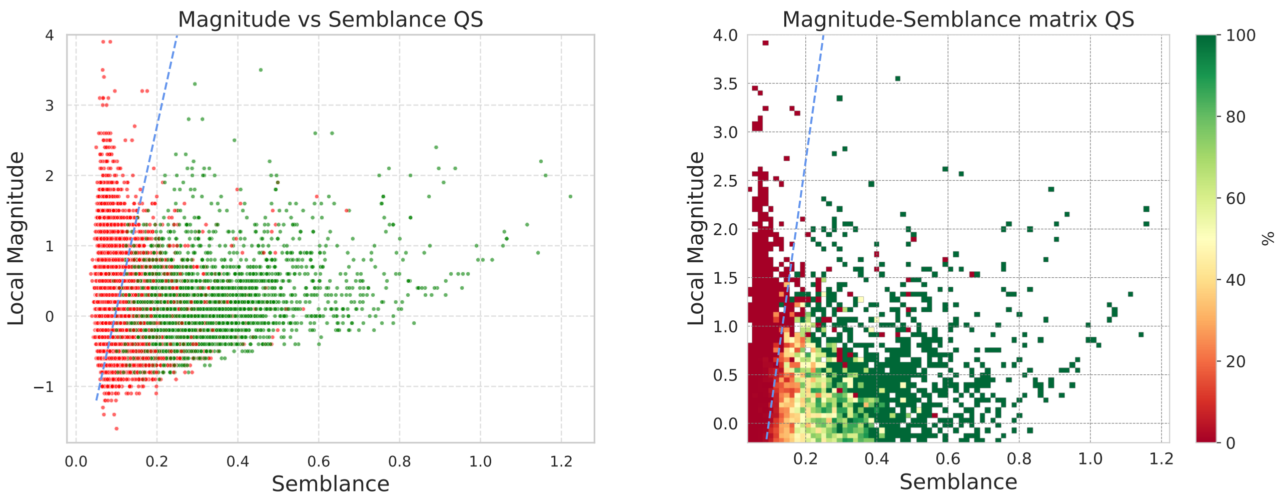

(a) **(b)**

Figure 1 Magnitude vs. QS semblance from the QS catalogs. a) earthquakes not present in the reference catalog are plotted as red dots, together with those that appear in both (green). The blue dashed line marks a possible boundary for low-semblance, high-magnitude dubious events. b) Magnitude-Semblance matrix calculated for the QS catalog. The color scale represents the ratio of green dots in each bin.

values. Conversely, larger events generally produce clearer signals at most stations, resulting in higher semblance values. Therefore, semblance is often indirectly correlated with earthquake magnitude through these effects. To prevent spurious detections due to very few stations, event detection requires a minimum of three stations; windows with fewer stations are discarded. The framework includes the calculation of local magnitudes using the method as for the PRN catalog (Bakun and Joyner, 1984). In this case, we consider only stations within 20 km of the epicenter for magnitude estimation. This choice arises because Qseek, by default, includes in the magnitude estimation all stations with SNR above a certain threshold (2 in our case) in the time window of the theoretical arrival, regardless of whether the station is triggered. For micro-earthquakes, distant stations often record mostly noise, which can be mistaken for seismic signal, leading to systematic overestimation — in comparison to the one of the same event in the reference CMS catalog — of local magnitude. Visual inspection of waveforms from distant stations confirms poor signal quality and random noise spikes causing false coherent signals. Given the network density, sufficient reliable stations are available within 20 km, so excluding more distant stations improves magnitude consistency and reliability for small events. This distance cutoff is not applied to the PRN workflow, which only considers triggered stations, thereby naturally filtering out noisy distant recordings. We verify that this approach results in more reliable local magnitudes for small events, while larger events are unaffected.

We then follow an approach similar to the PRN workflow to filter false positives and events with low-quality locations. We set the minimum number of picks to 5 to allow a recall aligned with PRN, at the cost of more false positives that will be filtered out later. This approach ensures a coherent comparison between the two methods while maximizing the recall of the reference catalog. Despite the preliminary filtering applied, the QS catalog still contains a significant number of false positives. These often correspond to events with higher magnitude (e.g., M $>$2) that are absent from the original catalog but with low semblance.

Given the size of the catalog, it is impractical to verify each earthquake manually. While a full manual labeling of true and false positives was not performed, a visual inspection of 100 randomly selected events from the initial catalog (consisting of 21,784 detections) was carried out to obtain a rough estimate of precision. Among these, 55 events were visually confirmed as true earthquakes, yielding an estimated precision of approximately 55% for the unfiltered catalog. This relatively low precision is an expected consequence of our deliberate choice to adopt low detection thresholds in the initial stage of the workflow, in order to maximize completeness and ensure that weak but potentially real events are not missed.

We propose an automated approach to filter false positives further. We compare detections in the QS and CMS catalogs. Specifically, we define a match if the origin time difference is less than 1.5 seconds and the epicentral distance is less than 10 km. Events appearing in both catalogs are considered true positives (TP). Those only appearing in QS may either be false positives or new detections. Plotting the two families of earthquakes in a Magnitude-Semblance diagram (Figure 1a) illustrates how TP (green dots) are clustered within a specific region of the graph, where the semblance correlates with the magnitude (Figure S1, Supplementary Information). Events with low semblance and high magnitude are believed to be false positives (Figure 1a).

Figure 1b shows the Magnitude-Semblance matrix for the QS catalog. The 2D magnitude-semblance space is rendered with pixels. The color scale represents the rate of green dots (ratio between the number of green detections and total detections in each Magnitude-Semblance cell) as a function of magnitude and semblance. The diagram shows only magnitudes equal to or higher than the magnitude of completeness estimated for the CMS catalog (-0.2), as we cannot compare those below this threshold.

Based on Figure 1, we propose the following empirical magnitude-semblance relation to filter false positives: $M = 26 \times S - 2.5$ (shown in the figure as a blue dashed line) where M is the magnitude and S is the semblance. The two coefficients were determined by grid search, minimizing the proportion of green events to the left of the line and the proportion of red events to its right. A higher weight (0.85) is assigned to the first proportion, as our primary objective is to maximize the recall from the reference catalog. Furthermore, red events are not necessarily false positives, but may also be new detections.

Following an approach similar to Adinolfi et al. (2018), we analyze the relationships between magnitude and average station-to-epicenter distance. Due to the attenuation experienced by the seismic waves with distance, low-magnitude earthquakes are more likely to be recorded by stations nearby. Therefore, detecting small-magnitude events with large average station-to-epicenter distances indicates false detections. Similarly to what we do in Figure 1, we determine an empirical relation to cut off false positives in external regions of Figure S2 (see Supplementary Information). After applying the magnitude–semblance filter, the catalog size was reduced to 11,399 events. This significant reduction, while discarding nearly half of the initial detections, is expected to improve the overall quality of the catalog by removing events with low signal coherence or insufficient magnitude. We repeat the visual check on 100 randomly selected samples. At this stage 78 events are confirmed, giving an estimated precision of 78%. The filtering step was therefore effective in balancing completeness and reliability, as confirmed by the substantial decrease in likely false positives and the retention of a large number of high-quality detections. The final value reflects the trade-off we chose between completeness and precision. While the general approach can also be used for other datasets, the obtained empirical relations are specific to the case study. We applied the same analysis to the PRN catalog for consistency, which showed fewer false positives (Figure S3, Supplementary Information). Figure S4 in the Supplementary Information shows some examples of waveforms corresponding to low magnitude earthquakes that passed the filter.

4 Results

The PRN catalog consists of 9,618 events, with a recall rate of 93%. The QS catalog consists of 11,399 earthquakes, with a recall rate of 77%. To assess the consistency between the catalogs, we analyze the time and locations of detected earthquakes, identifying matching patterns of epicenter clustering. Table 1 shows the median of the differences in origin time (Δt_o), epicentral location (Δloc_{epi}), hypocentral depth ($\Delta depth$), and local magnitude (ΔM_L) distributions, computed for each intersection between the catalogs.

Table 1 Median difference in origin time (Δt_o), epicentral location distance (Δloc_{epi}), hypocentral depth ($\Delta depth$), and local magnitude (ΔM_L) for same-event determinations in all pairs of catalogs.

$Catalog$	Δt_o	Δloc_{epi}	$\Delta depth$	ΔM_L
PRN-CMS	0.546 s	1.01 km	-0.18 km	-0.1
QS-CMS	0.515 s	1.34 km	-0.05 km	-0.1
QS-PRN	-0.016 s	1.01 km	0.09 km	-0.1

To assess location quality, we computed the median uncertainty and the 90th percentile for horizontal and vertical errors in each catalog. For the horizontal location error, the CMS catalog has a median of 0.4 km, with 90% of events located with uncertainty < 1.1 km (90th percentile of the uncertainty); PRN has a median of 1.1 km (90th percentile = 3.2 km), and QS a median of 0.2 km (90th percentile = 0.4 km). Regarding the vertical uncertainty, CMS and QS both show a median of 0.5 km (90th percentile = 1.1 km for both), while PRN has a median of 0.9 km (90th percentile = 2.1 km). The comparison between catalogs is also illustrated by the distribution of hypocenters with depth in the cross-sections of Figures 2a, 2b, 2c, while Figure 2d shows the size of the intersections (recall) between the catalogs and the new detections. The PRN catalog allows to identify structures where seismicity is clustered, due to the high quality of NonLinLoc locations. The majority of earthquakes are concentrated at the southwestern side of the basin (Monti della Maddalena Fault System) within the upper 10 km of the crust. At the same time, fewer events occur along the northeastern side, with greater depths.

The roughly oval shape of the epicentral distribution delimits the region where the network sensitivity is optimal (Morelli et al., 2025), and the domain of attention of approximately 3800 km^2, where the detection and location exercise has been limited (distributed seismicity extends further out). In agreement with the setup of the reference CMS catalog, we also exclude earthquakes with hypocenter depths larger than 23 km to focus on the shallow crustal domain of interest. New locations are primarily found in the same active region, where the new catalogs achieve detection of weaker earthquakes (Figure 3).

The normalized cumulative number of earthquakes in Figure 4 shows similar temporal evolutions of the three catalogs we compare. QS and PRN catalogs have comparable trends throughout the period considered, reflecting natural fluctuations in time of the seismic occurrence rate (note that cumulative distributions are all normalized to 1). The reference catalog's different time evolution (slightly flatter than QS and PRN at around 2021/09 and steeper at around 2023/05) might be the possible effect of parameter adjustments and optimization in the supervised monitoring routine.

Figure 5 shows the timeline of detected events and their magnitudes across the three catalogs. Overall, the

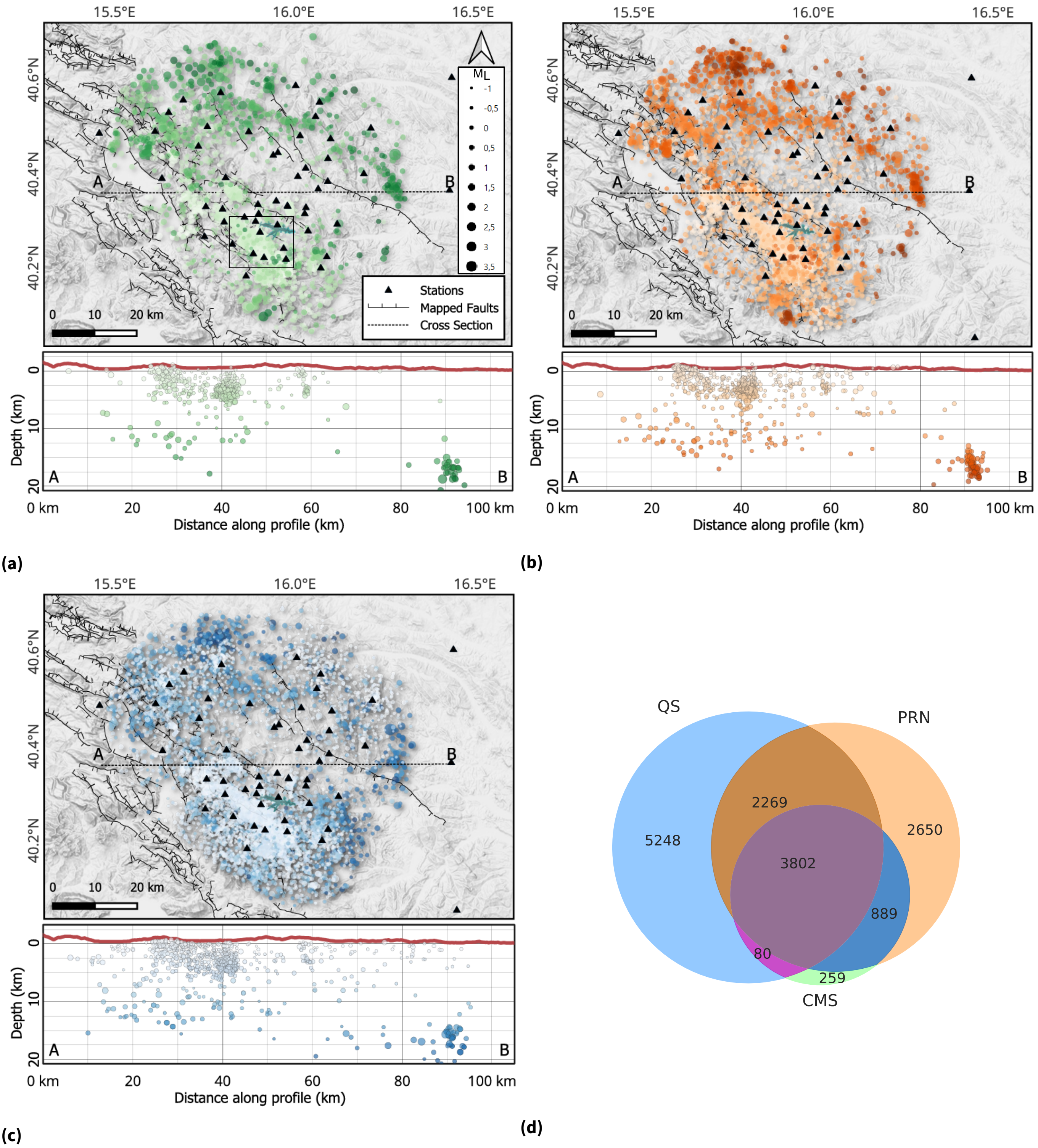

Figure 2 Distribution of epicenters and relative vertical cross sections for a) CMS catalog, b) PRN catalog, c) QS catalog. Vertical cross sections represent a sliver with a thickness of 5 km on each side. The dot size is proportional to Magnitude, while the color scales with the depth. Fault traces from the dataset by Lavecchia et al. (2023). The black rectangle around the Pertusillo lake area indicates the region selected for analysis in the Discussion section. d) Venn diagram of the three catalogs and their intersections. Green: reference CMS catalog, orange: PRN catalog, blue: QS catalog.

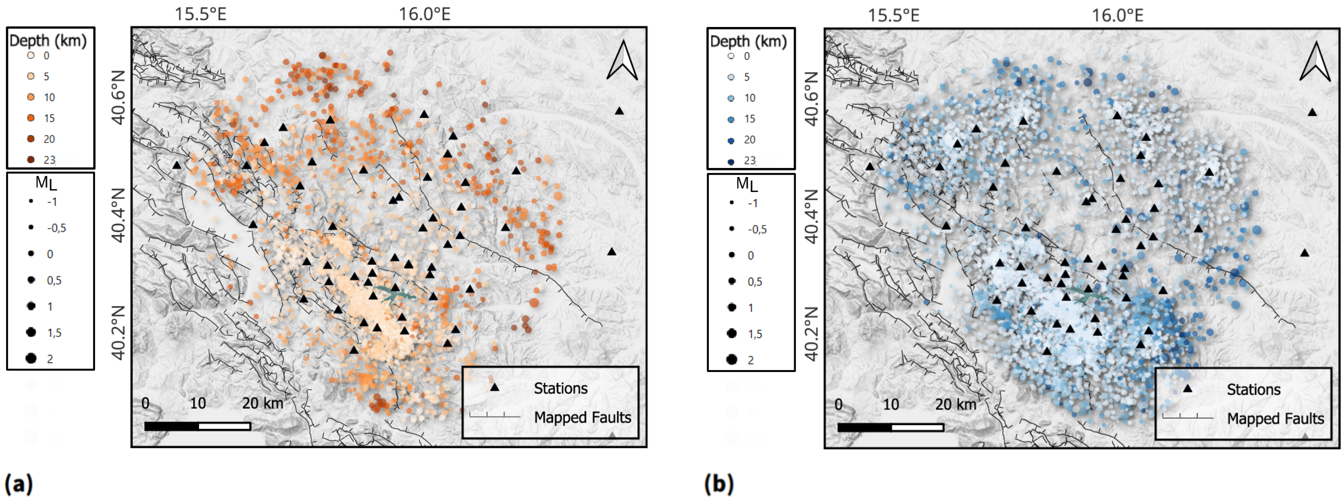

Figure 3 a) Epicenter distribution of earthquakes only present in the new PRN catalog and not in the reference bulletin. b) The epicenter distribution of earthquakes only present in the new QS catalog and not in the reference bulletin.

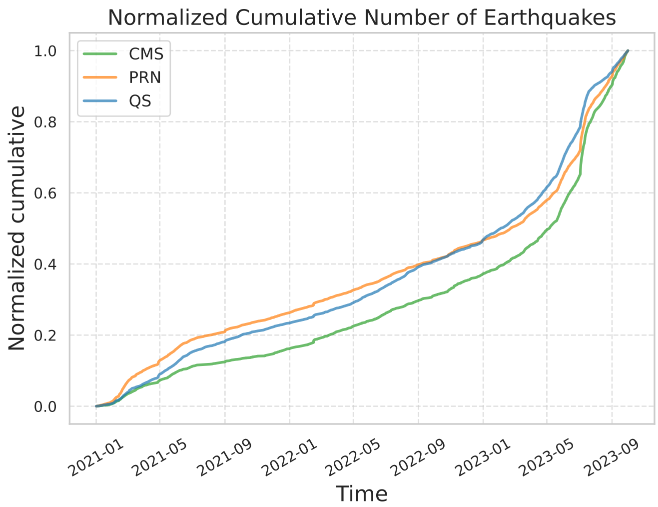

Figure 4 Normalized cumulative number of events as a function of time, compared for the three catalogs. Green: reference CMS catalog, orange: PRN catalog, blue: QS catalog.

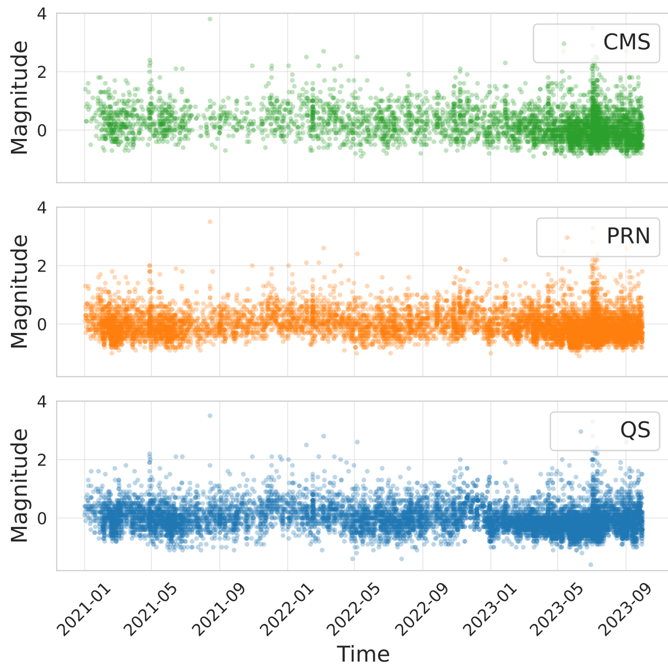

Figure 5 Distribution of magnitude of detected events in the three earthquake catalogs as a function of time. Green: reference CMS catalog, orange: PRN catalog, blue: QS catalog.

magnitude estimates and their temporal evolution are consistent among the catalogs. For larger events, the magnitude estimates remain in good agreement. The main differences appear at lower magnitudes, where both QS and PRN detect additional smaller events, effectively lowering the detection threshold. This difference becomes less significant over time, following a change in operational procedures on May 18, 2023, which improved the detection threshold in the reference CMS catalog.

Figure 5 shows that the rise in the number of events observed in 2023, along with larger magnitudes, reflects a general increase in seismic activity consistently captured by all three catalogs.

The frequency histogram shown in Figure 6 shows the distribution of local magnitude for the three catalogs. Similar to Figure 5, this demonstrates the improved performance of both new catalogs in the magnitude range -1 to 0.7. We estimate the completeness magnitude (M_c) with the Maximum Curvature method, and b-values with the Ogata and Katsura (1993) method. Results are presented in Table 2. M_c estimated for PRN and QS catalogs are lower than the reference bulletin (Table 2). Furthermore, we find consistent b-values close to 1 for PRN and QS, while the CMS catalog has a lower b-value. The discrepancy in few-unit counts at larger magnitude is due to (slightly) different magnitude estimates (as pointed out in the next Section) and to few events occurring near the border of the study area, which in different workflows may be located inside or outside the boundary (and be therefore excluded in one or another of the catalogs because of slightly different locations).

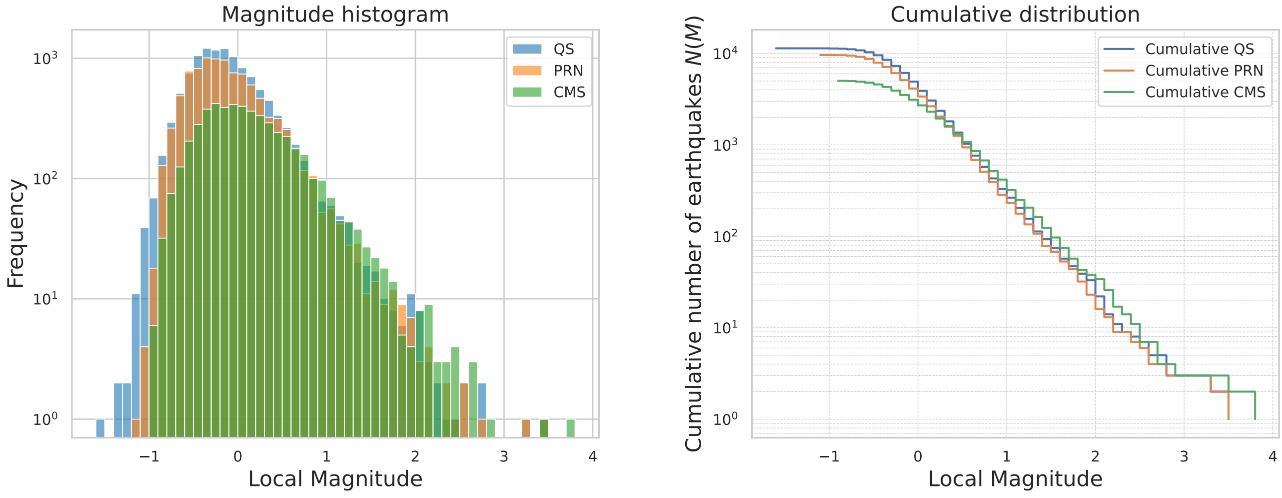

(a) **(b)**

Figure 6 a) Frequency histogram and b) cumulative distributions of the magnitude estimations for the three catalogs. Green: reference CMS catalog, orange: PRN catalog, blue: QS catalog.

Table 2 Completeness magnitude (MaxCurvature method) and *b* value for the three catalogs considered.

Catalog	M_c	*b* value
CMS	-0.2	0.93
PRN	-0.3	1.09
QS	-0.3	1.19

5 Discussion

5.1 Comparison of the workflows performance

Both machine learning-based methods exhibit remarkable efficiency in automatically monitoring the study area. The PRN method exhibits higher recall (93%) from the reference CMS catalog with accurate earthquake locations, resulting in better delineated seismic clusters and lineaments, as evidenced in map plots and cross sections (Figures 2 and 3). Although the absolute uncertainties from NonLinLoc are slightly larger, they provide a more reliable estimate of location accuracy due to the probabilistic nature of the algorithm, even when using a 1D velocity model. In contrast, the CMS catalog truncates hypocentral coordinates to fewer decimal places, reducing spatial resolution and limiting the ability to resolve small-scale structures illuminated by seismicity. The normalized cumulative event plots (Fig. 4) show similar trends. However, during the first period (before September 2021), the PRN and QS catalogs had a more rapid increase in the earthquake cumulative number than observed in the reference CMS detections. As the processing parameters for PRN and QS do not change with time, the elevated event rates before September 2021 may be due to increased small-magnitude seismicity that went unnoticed by the standard processing. This is shown in Figure 5, where many minor earthquakes are missing in the reference CMS catalog. Over time, this difference has become less pronounced due to a change in operational procedures, resulting in an improved detection threshold for the CMS. The supervised CMS routine has a sharp increase in event rate in August 2023 (Figure 5). This highlights an additional advantage of employing an efficient, automatic, and stable method for re-processing an entire period, ensuring consistency and reducing potential biases introduced by procedural changes over time.

We calculate local magnitudes in our methods using the same attenuation model as in the CMS catalog, but some small differences in the estimation remain. This explains the minor discrepancies in Figure 6. The same event can fall into two different histogram bins according to the catalog we are considering. This is hardly noticeable in more populated bins, but accounts for differences in bins with population on the scale of units. We attribute this to variance in the number of phases detected (and hence used for magnitude computation) for the same event in the three catalogs: PRN and QS events have more detected phases. This can be due to PhaseNet's higher sensitivity to finding more arrivals with lower amplitude than the original method. However, a more detailed comparison in magnitude estimation is outside the scope of this study. Regardless of these minor discrepancies in the histogram bins, we observe a higher number of earthquakes than the original catalog at low magnitude (between M_L -1 and 0.7), while preserving similarity between the two distributions at higher magnitudes. In Figure S5 (Supplementary Information) we compare only the events above a cutoff magnitude of the CMS catalog. This outcome aligns precisely with our objectives: enhancing the monitoring sensitivity to lower magnitudes, expecting similar results at higher magnitudes, thereby confirming the method's reliability.

5.2 Noise and performance of the detection

The distribution in time of the magnitude of earthquakes (Figure 5) shows coherent detection of the largest earthquakes as expected, and similar cyclic seasonal variations of the minimum magnitude detected in all the earthquake catalogs. This cyclicity is likely due to noise levels' seasonality, which can increase or reduce the SNR. The periods of lowest magnitude detected coincide with the summers, during which we expect lower noise levels related to calmer weather conditions. We are working in the frequency range 1 - 45 *Hz*, so we expect the contribution of sea noise and wind, which is likely a major contributor to noise at the highest frequencies. While in the range 1 - 10 *Hz* we expect the main contribution of anthropogenic noise. Both natural and anthropogenic noise sources, therefore, appear relevant in limiting seismic detection completeness. To analyse the possible correlation between the lowest magnitude detected and seismic noise, we calculate monthly PPSDs (Probabilistic Power Spectral Densities; McNamara and Boaz, 2005) at all stations. For each PPSD, we consider the median value in different frequency ranges. Many stations show a clear seasonality correlated with the variation of magnitude completeness, especially towards the lower end of the investigated frequency band. Figure 7a shows a station (GE.MARCO) exhibiting significant correlation (Pearson coefficient ~ 0.7, p-value « 0.05) between the PPSD median, computed in the frequency range 1 - 2 *Hz*, and the seasonal variation of the minimum magnitude in the PRN catalog. For readability purposes, we show here only one of the three catalogs; the results for the other two catalogs are provided in the Supplementary Information (Figure S6-S7).

A similar trend is found when we focus on the hourly variation. To investigate the influence of anthropogenic noise on our dataset we study the variation of the average minimum magnitude detected at different hours of the day: we found a diurnal oscillation with the highest value of such minimum detected magnitude (i.e., worst sensitivity, due to higher noise levels) at about 12 PM, and lowest values (best detection performance) detected around midnight. This diurnal oscillation well correlates with one of the median PPSD as shown in Fig. 7b for the same example station GE.MARCO (Pearson coefficient ~ 0.97, p-value « 0.05). The hourly median PPSD value is calculated by averaging the values over almost three years.

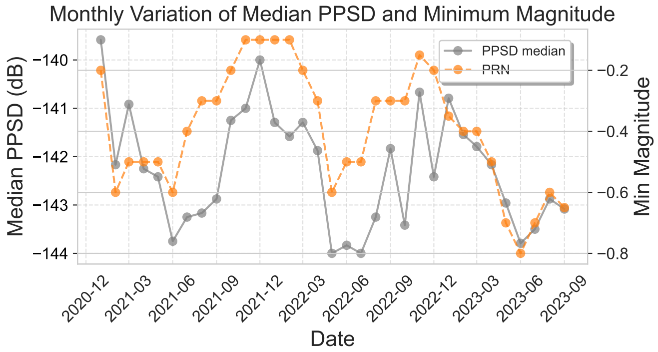

(a)

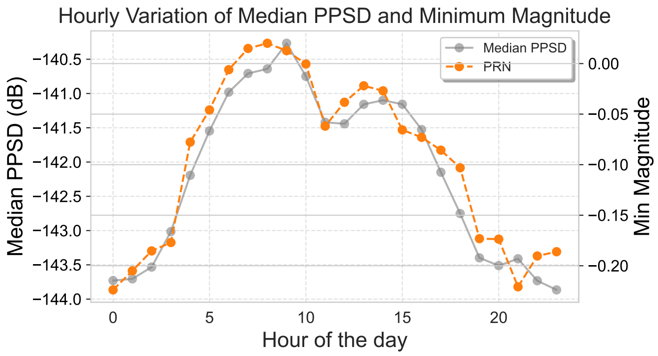

(b)

Figure 7 a) Monthly and b) hourly PPSD 50th percentile on a sample station (GE.MARCO) averaged over the three components (E, N, Z) vs minimum magnitude detected day by day. It is averaged over each month and hour, respectively.

5.3 Pertusillo water level and seismicity rate

With almost three years of data available, we may address the possible long-term modulation of the seismicity rate, in response to the seasonal changes of the water level at the Pertusillo artificial reservoir (Valoroso et al., 2009; Stabile et al., 2014). The reservoir has an average water depth of ∼95 m spanning an area of ∼75 km^2, experiencing significant and rapid seasonal water-level fluctuations (Valoroso et al., 2009). In such reservoirs, changing water levels change the stress within the surrounding rocks. During the loading phase, the fluid pressure within rock pores rises as the water level increases, which reduces the effective normal stress acting on fractures and faults. This stress can promote fault slip and increased seismicity. Conversely, during the unloading phase, when the water level drops, fluid pressure decreases, effective stress increases, and the seismicity rate tends to decline (e.g., Talwani, 1997; Gupta et al., 1972). Berbellini et al. (2021) found a significant correlation between relative seismic velocity variations and the hydrometric level of the nearby Agri river feeding the Pertusillo reservoir — considered a proxy for the total water storage in the shallow aquifers. The poroelastic effect likely governs the observed variations in seismicity rates, as fluctuations in water levels are mostly positively correlated with seismicity. Valoroso et al. (2023) points to such cyclicity over 13 years using a coarse reference catalog, while their local 13-month-long dataset does not allow for studying yearly cycles. Telesca et al. (2025) analyzed the temporal clustering of seismicity and its correlation with reservoir water level variations in the Pertusillo reservoir area using fractal and spectral analysis methods. Their findings suggest a delayed response of approximately 1 month, attributed to pore-pressure diffusion, supporting the hypothesis of protracted reservoir-triggered seismicity.

To verify such seasonal modulation in our dataset, we investigate a subset of the PRN catalog, limited to the region of interest closest to the lake (longitude 15.82-16.00, latitude 40.2-40.31), and compute the daily seismicity rate. The selected area is indicated by the black rectangle in Figure 2a. To exclude noise seasonality effects on the seismicity rate, we consider only the events above the magnitude of completeness Mc=-0.2, calculated with MaxCurvature method. In Figure 8 we compare such seismicity rate with the water level in the reservoir (downloaded from the district basin authority website: http://www.adb.basilicata.it). To preserve clarity and readability, we chose to display only one catalog; equivalent plots for the remaining two catalogs are included in the Supplementary Material (Figures S6-S7).

We observe a local increase in seismicity when the reservoir water level rises, and a corresponding decrease in seismicity when the water level falls, which is more notable in 2021 and 2023. The seasonal increase in seismicity occurs with a delay of some weeks. Notably, in 2023, we observed both the highest water levels and the highest seismicity rate. In contrast, during 2022, although the reservoir also reached high levels, the seismicity remained low and comparable to the background level, with only a slight and short-lived increase. Overall, the analysis of our more complete seismic catalog supports the hypothesized seasonal pattern of local seismicity (Valoroso et al., 2023).

6 Conclusions

Seismology is an excellent and promising field for the application of machine-learning (ML) methods for several purposes (e.g., Mousavi and Beroza, 2022, 2023b). Many applications have shown the ability to carry out complex tasks effectively and efficiently, so favourable operational developments are to be expected. Here, we have used the PhaseNet deep neural network seismic arrival time picking method (Zhu and Beroza, 2019), combined into two different workflows to analyse micro-seismicity recorded by a heterogeneous, integrated seismograph network in the tectonically active Val d'Agri region (Southern Italy), also seat of oil and gas extraction as well as artificial water impoundment. Compared to a more customary reference practice based on an STA/LTA detector and manual operator revision, the ML-based workflows produced rich earthquakes catalogs with about twice the number of events and twice the detected arrivals per event (a larger number of phases to be used in the hypocentral location is highly beneficial for its quality). As illustrated in the Methods section, we completed our workflows using an efficient method to discard false positives.

We chose a rather conservative detector setup that reproduces most of the events in the reference catalog (PRN: recall rate 93%; QS: 77%) while discarding many false positives and uncertain events.

The benefit of the automatically generated catalogs is apparent. Once the significant parameters (such as the minimum number of detected phases to allow the definition of an event, and similar criteria) are set, the workflow can be applied automatically to real-time data. Besides the apparent advantage of a high saving of operator time, this fact also contributes to the homogeneity of results, as with the wish of any different parameter value, an entire catalog can be recomputed on the fly.

By increasing the sensitivity of the event detection process, we may more easily see the influence of time variations on the population of earthquakes. Furthermore, we can detect the impact of the seasonal variations of high-frequency background seismic noise connected with weather, and we distinctly see a correlation of micro-earthquake occurrence with the charge-discharge cycles of the Pertusillo water reservoir. Although these observations suggest a correlation, further investigation is required to fully understand the relationship between water level fluctuations and seismicity rates. Using the PRN catalog, future studies will focus on a more detailed analysis of the temporal and spatial patterns of seismic activity in response to changes in water levels, particularly considering poroelastic effects and delayed responses. This upcoming research will aim to quantify these correlations more rigorously and provide deeper insights into the mechanisms driving the observed seismic behavior.

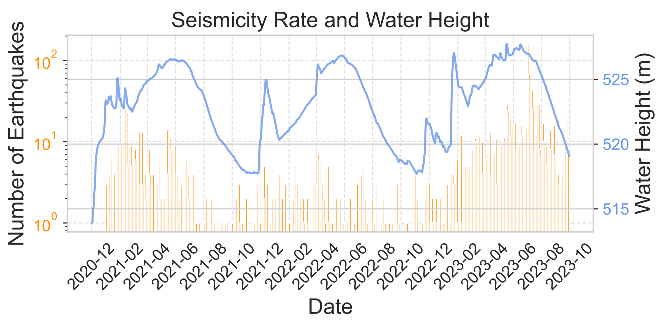

Figure 8 Pertusillo lake water level over time (blue) vs number of earthquakes every 3 days (orange) in the PRN catalog, i.e., seismicity rate. Water level data starts in December 2020, considering the delayed effect of seismicity.

Data and code availability

We used open seismic data from the following seismic networks: IV (Istituto Nazionale di Geofisica e Vulcanologia – INGV, 2005, doi:10.13127/SD/X0FXNH7QFY), VD (CNR IMAA Consiglio Nazionale delle Ricerche - Italy, 2019, https://doi.org/10.7914/SN/VD, Stabile et al., 2020), IX (Irpinia Seismic Network – ISNet, 2005) and GE (GEOFON Data Centre, 1993, https://doi.org/10.14470/TR560404). Waveforms and metadata can be accessed through the Federation of Digital Seismograph Networks Web services at GEOFON (https://geofon.gfz.de/waveform/webservices/) and INGV (/https://terremoti.ingv.it/webservices_and_software).

Seismic data from networks VA (ENI SpA, 2001, https://doi.org/10.7914/SN/VA) and TP (TOTAL E&P Italia Spa, 2018, https://www.fdsn.org/networks/detail/TP/) must be requested from the operators.

Software PhaseNet is published on GitHub https://github.com/AI4EPS/PhaseNet. Software REAL is available at https://github.com/Dal-mzhang/REAL. Software NonLinLoc is available at https://github.com/ut-beg-texnet/NonLinLoc. Qseek is published on GitHub https://github.com/pyrocko/qseek.

We used Obspy (Beyreuther et al., 2010) and Pyrocko (Heimann et al., 2017) libraries for data analysis. Plots have been generated using Matplotlib (Hunter, 2007), and maps using QGIS.

The PRN and QS catalogs are available on Zenodo.org (doi:10.5281/zenodo.17123383 (Caredda et al., 2025)).

7 Acknowledgements

We express our sincere gratitude to the CMS analysts and board for providing the data and facilitating this research. Special thanks to Spina Cianetti for the initial guidance on software usage. We also extend our appreciation to all network operators for maintaining the seismic instrumentation utilized in this study; particularly commercial operators ENI and Total E&P for sharing their interest in our research, providing ongoing support, and collaborating with us. We also thank the editor and the anonymous reviewers for their constructive comments and suggestions, which helped improve the quality of this manuscript.

Competing interests

The authors acknowledge that there are no conflicts of interest recorded.

References

Adinolfi, G., Cesca, S., Picozzi, M., Heimann, S., and Zollo, A. Detection of weak seismic sequences based on arrival time coherence and empiric network detectability: an application at a near fault observatory. *Geophys. J. Int.*, (218):2054–2065, 2018.

Allen, R. Automatic earthquake recognition and timing from single traces. *Bulletin of the Seismological Society of America*, 68(5): 1521–1532, 1978. doi: 10.1785/BSSA0680051521.

Bakun, W. and Joyner, W. The ML Scale in Central California. *Bulletin of the Seismological Society of America*, 75(5):1827–1843, 1984.

Berbellini, A., Zaccarelli, L., Faenza, L., Garcia, A., Improta, L., De Gori, P., and Morelli, A. Effect of Groundwater on Noise-Based Monitoring of Crustal Velocity Changes Near a Produced Water Injection Well in Val d'Agri (Italy). *Frontiers in Earth Science*, 9, 2021. doi: 10.3389/feart.2021.626720.

Beyreuther, M., Barsch, R., Krischer, L., Megies, T., Behr, Y., and Wassermann, J. ObsPy: A Python Toolbox for Seismology. *Seismological Research Letters*, 81(3):530–533, 2010.

Braun, T., Danesi, S., and Morelli, A. Application of monitoring guidelines to induced seismicity in Italy. *Journal of Seismology*, pages 1–14, 2020. doi: 10.1007/s10950-019-09901-7.

Caredda, E., Isken, M. P., Cesca, S., Errico, M., Zerbinato, G., and Morelli, A. Earthquake catalogs for: Improving detection of micro-earthquakes in the Val d'Agri region (Southern Italy) using Deep Learning algorithms, Sept. 2025.

Cello, G., Tondi, E., Micarelli, L., and Mattioni, L. Active tectonics and earthquake sources in the epicentral area of the 1857 Basilicata earthquake, southern Italy. *J. Geodyn.*, 36(19):37–50, 2003.

Cianetti, S., Lomax, A., Michelini, A., and et al. Comparison of Deep-Learning Versus Manual Seismic Arrival-Time Picks Based on Quality of High-Precision Earthquake Locations and Seismic Tomography., 2025.

Dziewonski, A. M. and Anderson, D. L. Preliminary reference Earth model. *Physics of the earth and planetary interiors*, 25(4): 297–356, 1981.

Fonzetti, R., Govoni, A., De Gori, P., and Chiarabba, C. A rapid analysis of aftershock processes after a moderate magnitude earthquake with ML methods. *Geophysical Journal International*, 239 (1):99–111, 2024. doi: https://doi.org/10.1093/gji/ggae262.

Grigoli, F., Cesca, S., Amoroso, O., Emolo, A., Zollo, A., and Dahm, T. Automated seismic event location by waveform coherence analysis. *Geophysical Journal International*, 196(3):1742–1753, 2014. doi: https://doi.org/10.1093/gji/ggt477.

Gupta, H., Rastogi, B. K., and Narain, H. Common features of the reservoir-associated seismic activities. *Bulletin of the Seismological Society of America*, 62(2):481–492, 1972. doi: https://doi.org/10.1093/gji/ggt477.

Heimann, S., Kriegerowski, M., Isken, M., Cesca, S., Daout, S., Grigoli, F., Juretzek, C., Megies, T., N., N., Steinberg, A., Sudhaus, H., Vasyura-Bathke, H., Willey, T., and Dahm, T. Pyrocko - An open-source seismology toolbox and library, 2017.

Hunter, J. D. "Matplotlib: A 2D Graphics Environment". *Computing in Science & Engineering*, 9(3):90–95, 2007.

Improta, L., Bagh, S., De Gori, P., Valoroso, L., Pastori, M., Piccinini, D., Chiarabba, C., Anselmi, M., and Buttinelli, M. Reservoir structure and wastewater-induced seismicity at the Val d'Agri Oilfield (Italy) shown by three-dimensional v_P and v_P/v_S local earthquake tomography. *J. Geophys. Res.*, 122(11):9050–9082, 2017. doi: https://doi.org/10.1002/2017JB014725.

Isken, M., Niemz, P., Münchmeyer, J., Büyükakpınar, P., Heimann, S., Cesca, S., Vasyura-Bathke, H., and Dahm, T. Qseek: A data-driven Framework for Automated Earthquake Detection, Localization and Characterization. *Seismica*, 4(1), 2025. doi: https://doi.org/10.26443/seismica.v4i1.1283.

Lavecchia, G., Bello, S., Cirillo, D., Pietrolungo, F., and Brozzetti, F. Quaternary-Host Faults Database 2.0 (Southern Italy) [Data set], 2023.

Lomax, A., Virieux, J., Volant, P., and Berge-Thierry, C. *Probabilistic Earthquake Location in 3D and Layered Models.*, volume 18, pages 101–134. Springer, Dordrecht, 2000. doi: https://doi.org/10.1007/978-94-015-9536-0_5.

Lomax, A., Michelini, A., and Curtis, A. *Earthquake Location, Direct, Global-Search Methods.*, volume 18. Springer, New York, NY., 2014. doi: https://doi.org/10.1007/978-94-015-9536-0_5.

McNamara, D. E. and Boaz, R. I. Seismic Noise Analysis System Using Power Spectral Density Probability Density Functions: A Stand-Alone Software Package. *USGS Open-File Report*, 1438, 2005.

Michelini, A., Cianetti, S., Gaviano, S., Giunchi, C., Jozinović, D., and Lauciani, V. INSTANCE – the Italian seismic dataset for machine learning. *Earth System Science Data*, 13(12):5509–5544, 2021. doi: 10.5194/essd-13-5509-2021.

Morelli, A., Anselmi, M., Braun, T., Danesi, S., Errico, M., Famiani, D., Garcia, A., Molinari, I., Vassallo, M., Zaccarelli, L., and Zerbinato, G. A state-of-the-art analysis system designed to monitor microseismicity at a local scale. *Annals of Geophysics*, 67(6), 2025. doi: https://doi:10.4401/ag-9124.

Mousavi, S. and Beroza, G. Deep-learning seismology. *Science*, 377 (1), 2022. doi: 10.1126/science.abm4470.

Mousavi, S., Ellsworth, W., Zhu, W., and et al. Earthquake transformer—an attentive deep-learning model for simultaneous earthquake detection and phase picking. *Nat Commun*, 11 (3952), 2020. doi: https://doi.org/10.1038/s41467-020-17591-w.

Mousavi, S. M. and Beroza, G. C. Bayesian-Deep-Learning Estimation of Earthquake Location From Single-Station Observations. *IEEE Transactions on Geoscience and Remote Sensing*, 58 (11):8211–8224, 2020. doi: 10.1109/TGRS.2020.2988770.

Mousavi, S. M. and Beroza, G. C. Machine Learning in Earthquake Seismology. *Annual Review of Earth and Planetary Sciences*, 51(Volume 51, 2023):105–129, 2023a. doi: https://-

doi.org/10.1146/annurev-earth-071822-100323.

Mousavi, S. M. and Beroza, G. C. Machine Learning in Earthquake Seismology. *Annual Review of Earth and Planetary Sciences*, 51(1):105–129, 2023b. doi: https://doi.org/10.1146/annurev-earth-071822-100323.

Ogata, Y. and Katsura, K. Analysis of temporal and spatial heterogeneity of magnitude frequency distribution inferred from earthquake catalogues. *Geophysical Journal International*, 113(3):727–738, 1993. doi: https://doi.org/10.1111/j.1365-246X.1993.tb04663.x.

Richards-Dinger, K. B. and Shearer, P. M. Earthquake locations in southern California obtained using source-specific station terms. *Journal of Geophysical Research: Solid Earth*, 105(B5): 10939–10960, May 2000. doi: 10.1029/2000JB900014.

Stabile, T., Giocoli, A., Lapenna, V., Perrone, A., Piscitelli, S., and Telesca, L. Evidence of Low-Magnitude Continued Reservoir-Induced Seismicity Associated with the Pertusillo Artificial Lake (Southern Italy). *Bulletin of the Seismological Society of America*, 104(4):1820–1828, 2014. doi: 10.1785/0120130333.

Stabile, T., Serlenga, V., Satriano, C., Romanelli, M., Gueguen, E., Gallipoli, M. R., Ripepi, E., Saurel, J.-M., Panebianco, S., Bellanova, J., and Enrico Priolo, E. The INSIEME seismic network: a research infrastructure for studying induced seismicity in the High Agri Valley (southern Italy). *Earth System Science Data*, 12 (1):519–538, 2020. doi: 10.5194/essd-12-519-2020.

Talwani, P. On the Nature of Reservoir Induced Seismicity. *Pure and Applied Geophysics*, 150:473–492, 1997. doi: 10.1785/0120130333.

Telesca, L., Panebianco, S., Serlenga, V., and Stabile, T. A. Fractal, Spectral, and Topological Analysis of the Reservoir-Induced Seismicity of Pertusillo Area (Southern Italy). *Fractal and Fractional*, 9(4), 2025.

Vaezi, Y. and van der Baan, M. Comparison of the STA/LTA and power spectral density methods for microseismic event detection. *Geophysical Journal International*, 203(3):1896–1908, 2015. doi: https://doi.org/10.1093/gji/ggv419.

Valoroso, L., Improta, L., Chiaraluce, L., Di Stefano, R., Ferranti, L., Govoni, A., and Chiarabba, C. Active faults and induced seismicity in the Val d'Agri area (Southern Apennines, Italy). *Geophysical Journal International*, 178(1):488–502, 2009. doi: https://doi.org/10.1111/j.1365-246X.2009.04166.x.

Valoroso, L., Piccinini, D., Improta, L., Gaviano, S., and Giunchi, C. Characterizing seismogenic fault structures of the Lake Pertusillo reservoir induced seismicity (Southern Italy) using a relocated template-matching catalog. *Journal of Geophysical Research: Solid Earth*, 128, e2022JB025879:488–502, 2023. doi: https://doi.org/10.1029/2022JB025879.

Wickham-Piotrowski, A., Font, Y., Regnier, M., Delouis, B., Lengliné, O., Segovia, M., and Bletery, Q. Achieving a Comprehensive Microseismicity Catalog through a Deep-Learning-Based Workflow: Applications in the Central Ecuadorian Subduction Zone. *Bulletin of the Seismological Society of America*, 114(2):823–841, 12 2023. doi: 10.1785/0120230128.

Woollam, J., Münchmeyer, J., Tilmann, F., Rietbrock, A., Lange, D., Bornstein, T., Diehl, T., Giunchi, C., Haslinger, F., Jozinović, D., Michelini, A., Saul, J., and Soto, H. SeisBench—A Toolbox for Machine Learning in Seismology. *Seismological Research Letters*, 93(3):1695–1709, 03 2022. doi: 10.1785/0220210324.

Zhang, M., Ellsworth, W., and Beroza, G. Rapid Earthquake Association and Location. *Seismological Research Letters*, 90(6): 2276–2284, 2019. doi: 10.1785/0220190052.

Zhu, W. and Beroza, G. PhaseNet: a deep-neural-network-based seismic arrival-time picking method. *Geophysical Journal International*, 216(1):261–273, 2019. doi: 10.1093/gji/ggy423.

Zhu, W., Hou, A. B., Yang, R., Datta, A., Mousavi, S. M., Ellsworth, W. L., and Beroza, G. C. QuakeFlow: a scalable machine-learning-based earthquake monitoring workflow with cloud computing. *Geophysical Journal International*, 232(1):684–693, 09 2022a. doi: 10.1093/gji/ggac355.

Zhu, W., McBrearty, I. W., Mousavi, S. M., Ellsworth, W. L., and Beroza, G. C. Earthquake Phase Association Using a Bayesian Gaussian Mixture Model. *Journal of Geophysical Research: Solid Earth*, 127(5):e2021JB023249, 2022b. doi: https://doi.org/10.1029/2021JB023249.